

Atomic Transit and Delayed Ionization Effects
on Cesium Beam Frequency Standards

AD-A196 216

Prepared by
B. JADUSZLIWER
Chemistry and Physics Laboratory
Laboratory Operations
The Aerospace Corporation
El Segundo, CA 90245

12 May 1988

Prepared for
SPACE DIVISION
AIR FORCE SYSTEMS COMMAND
Los Angeles Air Force Base
P.O. Box 92960, Worldway Postal Center
Los Angeles, CA 90009-2960

APPROVED FOR PUBLIC RELEASE;
DISTRIBUTION UNLIMITED

DTIC
SELECTED
JUN 20 1988
S H D

This report was submitted by The Aerospace Corporation, El Segundo, CA 90245, under Contract No. F04701-85-C-0086 with the Space Division, P.O. Box 92960, Worldway Postal Center, Los Angeles, CA 90009-2960. It was reviewed and approved for The Aerospace Corporation by S. Feuerstein, Director, Chemistry and Physics Laboratory.

Lt Michael J. Mitchell was the Air Force project officer.

This report has been reviewed by the Public Affairs Office (PAS) and is releasable to the National Technical Information Service (NTIS). At NTIS, it will be available to the general public, including foreign nationals.

This technical report has been reviewed and is approved for publication. Publication of this report does not constitute Air Force approval of the report's findings or conclusions. It is published only for the exchange and stimulation of ideas.

Michael J. Mitchell

MICHAEL J. MITCHELL, Lt, USAF
MOIE Project Officer
SD/CWNZS

Raymond M. Leong

RAYMOND M. LEONG, Major, USAF
Deputy Director, AFSTC West Coast Office
AFSTC/WCO OL-AB

UNCLASSIFIED

SECURITY CLASSIFICATION OF THIS PAGE

REPORT DOCUMENTATION PAGE

1a. REPORT SECURITY CLASSIFICATION Unclassified			1b. RESTRICTIVE MARKINGS			
2a. SECURITY CLASSIFICATION AUTHORITY			3. DISTRIBUTION / AVAILABILITY OF REPORT Approved for public release; distribution unlimited.			
2b. DECLASSIFICATION / DOWNGRADING SCHEDULE						
4. PERFORMING ORGANIZATION REPORT NUMBER(S) TR-0086A(2470-03)-2			5. MONITORING ORGANIZATION REPORT NUMBER(S) SD-TR-88-57			
6a. NAME OF PERFORMING ORGANIZATION The Aerospace Corporation Laboratory Operations		6b. OFFICE SYMBOL (If applicable)		7a. NAME OF MONITORING ORGANIZATION Space Division		
6c. ADDRESS (City, State, and ZIP Code) El Segundo, CA 90245			7b. ADDRESS (City, State, and ZIP Code) Los Angeles Air Force Base Los Angeles, CA 90009-2960			
8a. NAME OF FUNDING / SPONSORING ORGANIZATION		8b. OFFICE SYMBOL (If applicable)		9. PROCUREMENT INSTRUMENT IDENTIFICATION NUMBER F04701-85-C-0086		
8c. ADDRESS (City, State, and ZIP Code)			10. SOURCE OF FUNDING NUMBERS			
			PROGRAM ELEMENT NO.	PROJECT NO.	TASK NO.	WORK UNIT ACCESSION NO.
11. TITLE (Include Security Classification) Atomic Transmit and Delayed Ionization Effects on Cesium Beam Frequency Standards						
12. PERSONAL AUTHOR(S) Jaduszliwer, Bernardo						
13a. TYPE OF REPORT		13b. TIME COVERED FROM _____ TO _____		14. DATE OF REPORT (Year, Month, Day) 1988 May 12		15. PAGE COUNT 26
16. SUPPLEMENTARY NOTATION						
17. COSATI CODES			18. SUBJECT TERMS (Continue on reverse if necessary and identify by block number)			
FIELD	GROUP	SUB-GROUP	Atomic Clock, Cesium Beam Frequency Standard, Atomic Beam Modulation, (1)			
19. ABSTRACT (Continue on reverse if necessary and identify by block number)						
<p>In a compact cesium beam atomic clock, the magnets that perform state selection and analysis transmit a narrow slice of the Maxwellian velocity distribution leaving the cesium oven. Increasing the width of the transmitted velocity distribution will increase the beam intensity, and thus the clock's signal-to-noise ratio, but it will also distort the atomic beam amplitude modulation, which gives the clock error signal, and thus reduce the signal-to-noise ratio. Detection is accomplished by surface ionization on a hot wire, which acts as a low-pass filter. The combined effects of these processes on the clock's error signal are analyzed in detail for a test case involving an atomic beam which has been square-wave amplitude-modulated by its interaction with the frequency-modulated microwave field. While our analysis has been performed for the type of compact cesium beam tube used on board Global Positioning System satellites, its most general conclusions are valid for any atomic beam passive-frequency standard and show the importance of processes taking place after the atom-microwave interaction is completed for the optimization of the clock's performance.</p>						
20. DISTRIBUTION / AVAILABILITY OF ABSTRACT <input checked="" type="checkbox"/> UNCLASSIFIED/UNLIMITED <input type="checkbox"/> SAME AS RPT <input type="checkbox"/> DTIC USERS				21. ABSTRACT SECURITY CLASSIFICATION Unclassified		
22a. NAME OF RESPONSIBLE INDIVIDUAL			22b. TELEPHONE (Include Area Code)		22c. OFFICE SYMBOL	

DD FORM 1473, 84 MAR

83 APR edition may be used until exhausted
All other editions are obsolete.

SECURITY CLASSIFICATION OF THIS PAGE

UNCLASSIFIED

PREFACE

The author would like to thank Drs. R. Frueholz, S. Karuza, and Mr. W. Johnson for some illuminating discussions regarding this work.



Accession For	
NTIS GRA&I	<input checked="" type="checkbox"/>
DTIC TAB	<input type="checkbox"/>
Unannounced	<input type="checkbox"/>
Justification	
By	
Distribution/	
Availability Codes	
Avail and/or	
Dist	Special
A-1	

CONTENTS

I.	INTRODUCTION.....	5
II.	IONIZER EFFECTS.....	9
III.	WAVEFORM DISTORTION.....	15
IV.	INTENSITY EFFECTS.....	21
V.	CONCLUSIONS.....	25
	REFERENCES.....	29

FIGURES

1.	Ionic Dwell Time vs. Tungsten Wire Inverse Absolute Temperature.....	10
2.	Response of Ionizer to an Incident Amplitude-modulated Atomic Beam.....	12
3.	Amplitude-modulated Waveforms, Normalized by I_0	17
4.	Amplitude-modulated Waveforms, Normalized by I_0	18
5.	Magnitude of Detected Error Signal per Unit Beam Intensity vs. Width of Velocity Distribution.....	19
6.	Magnitude of Detected Error Signal per Unit Beam Intensity vs. Depth of Beam Amplitude Modulation.....	19
7.	Signal and Signal-to-Noise Ratio (in Arbitrary Units) vs. Width of Velocity Distribution.....	23
8.	Magnitude of Detected Error Signal per Unit Beam Intensity vs. Modulation Frequency.....	26

I. INTRODUCTION

In this report we discuss some effects on cesium beam clock performance of atomic transit times after microwave interrogation and detector response times. We will refer to these combined processes as the effects of the "post-microwave segment" of the cesium beam tube. Our analysis has been conducted for the type of compact cesium beam tubes used on Global Positioning System (GPS) satellites, but its most general conclusions are valid for any atomic beam passive frequency standard.

In compact cesium beam atomic clocks, the atomic beam is detected by surface ionization on a hot wire, and hyperfine state preparation and analysis are accomplished by atomic deflection in strongly inhomogeneous magnetic fields. Since atomic deflection in a magnetic field gradient is velocity-dependent, only atoms within a relatively narrow range of speeds will follow trajectories leading from the cesium oven, through the state-selecting magnet, the Ramsey cavity, and the state-analyzing magnet, to the detector; the cesium beam tube acts as its own passband velocity filter, and its geometry determines the velocity distribution of the detected atoms.

Two independent processes will tend to smear out the time-dependent component of the atomic beam signal introduced by microwave frequency modulation. First, atoms leaving the microwave interrogation volume simultaneously with different speeds will arrive at the ionizer at different times; the spread in arrival times Δt_A will be determined by the atomic beam velocity spread Δv . Second, atoms arriving at the ionizer simultaneously will leave as ions with an exponential distribution of residence times characterized by a temperature- and material-dependent ionic dwell time τ . These two processes will introduce a significant smearing of the time-dependent component of the atomic beam signal if either one (or both) of Δt_A and τ are comparable to $T_m/2\pi$, where $T_m = 1/\nu_m$ is the modulation period. The relative importance of these two processes will be determined by the relative length of Δt_A and τ .

The discriminator function of the atomic system is determined primarily by the atomic resonance lineshape and the microwave modulation scheme, since taken together, these two will determine how microwave detuning is translated

into intensity modulation of the atomic beam. However, the intensity modulation impressed upon the atomic beam by microwave interrogation will be degraded during transit and detection by the aforementioned processes, leading in turn to the degradation of the discriminator function. Thus, the choice of modulation frequency for best clock performance will not only depend on the atomic resonance lineshape, but also on the atomic velocity distribution and the choice of ionizer material and operating temperature.

We have modeled quantitatively the effects of the smearing of the time-dependent components of the beam signal by both the spreads in atomic transit and ion residence times for a test case in which the intensity of the state-selected atomic beam is square-wave amplitude modulated by its sequential interactions with the microwave field and the inhomogeneous field of the state-analyzer magnet. The modulated atomic beam intensity at the exit of the Ramsey cavity within the tube of trajectories leading to the detector is given by

$$I(t) = I_0 \quad nT_m \leq t < (n+1/2) T_m \quad (1a)$$

$$I(t) = I_0(1-d) \quad (n+1/2) T_m \leq t < (n+1) T_m \quad (1b)$$

where n is any integer and d the depth of amplitude modulation ($0 \leq d \leq 1$). The average atomic beam intensity is given by $\langle I \rangle = I_0 (d-1/2)$. This is the type of intensity modulation that would be achieved if the microwaves fed into the Ramsey cavity underwent square-wave frequency modulation and their average frequency was different from the atomic transition frequency, $\nu \neq \nu_0$. The depth of amplitude modulation d will in general depend on the microwave detuning, the depth of frequency modulation, and the atomic transition lineshape. In most of what follows we will be taking $d = 1$ for clarity. This is obviously unrealistic, but does not entail a loss of generality since the results of our modeling scale linearly with d , as we will show later.

The atomic beam intensity incident on the detector will be given by $I'(t)$, and $I_+(t)$ will be the ion current (ions/s) emerging off the ionizer surface. If $I(t)$ is periodic of period T_m , so will be $I'(t)$ and $I_+(t)$. Also, $\langle I_+ \rangle = \epsilon \langle I' \rangle = \epsilon \langle I \rangle$, where ϵ is the hot-wire ionization efficiency.

We will assume for our test case that the time-dependent component of the atomic beam signal is detected by a phase sensitive technique, using as reference $R(t-t_0)$, a unit amplitude square wave of the same frequency as the atomic beam modulation, where t_0 is introduced to provide a suitable phase-shift. The magnitude of the error signal will be proportional to

$$|E| = \frac{1}{T_m} \int_0^{T_m} |I_+(t) - \langle I_+ \rangle| dt \quad (2)$$

and its sign will depend on whether $I_+(t)$ and $R(t-t_0)$ are in phase or in phase opposition. Typically, the amplified ion signal would be filtered before phase-sensitive detection. Incorporating the filter into our model would change the results somewhat, but our conclusions would remain valid.

II. IONIZER EFFECTS

The ion evaporation rate I_+ at the ionizer surface can be expressed as

$$I_+ = \gamma N_+ \quad (3)$$

where N_+ is the total number of cesium ions on the ionizer surface, and γ the ionic evaporation probability per unit time. This assumes fairly low ion-surface concentrations, so that the evaporation rate will be characteristic of the ion-surface binding, without regard to ion-ion or ion-neutral cesium interaction on the surface.

The mean life (or dwell time) of the adsorbed ions is given by $\tau = 1/\gamma$, and Hughes and Levinstein¹ have shown that, in general, the temperature dependence of τ is given by

$$\tau = \tau_\infty \exp(Q_+/kT) \quad (4)$$

which can be understood in terms of noninteracting particles trapped behind a potential barrier of height Q_+ (the ionic heat of desorption). Nazarov² studied atomic and ionic desorption dynamics for the cesium-tungsten system, and from his work $\tau_\infty \cong 7.9 \times 10^{-12}$ s; $Q_+ \cong 1.84$ eV. Figure 1 shows the dwell time τ versus temperature for cesium ions on a tungsten surface, calculated using Eq. (4) with Nazarov's results. For comparison purposes, it also shows τ for rubidium ions on tungsten, as measured by Hughes and Levinstein.¹ For our test case, we are assuming a tungsten ionizer operated at $T = 1220$ K, yielding $\tau \cong 3 \times 10^{-4}$ s.

If $I'(t)$ is the atomic current impinging on the ionizer, the ion current satisfies

$$\tau \frac{dI_+}{dt} + I_+ = \epsilon I'(t) \quad (5)$$

where, typically, $\epsilon \cong 1$.

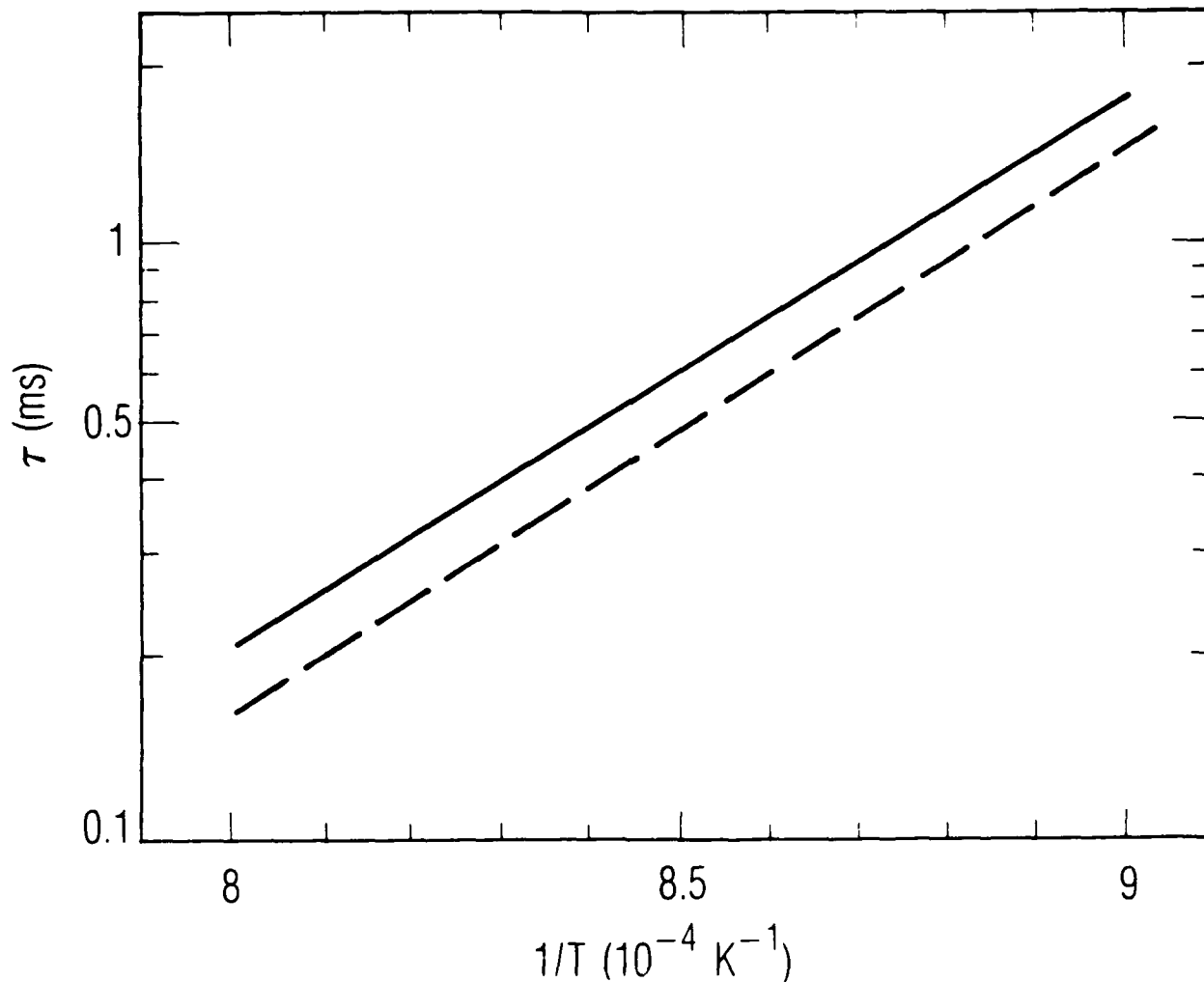


Fig. 1. Ionic Dwell Time vs. Tungsten Wire Inverse Absolute Temperature. Solid line: Cesium, from Nazarov.²
Dashed line: Rubidium, from Hughes and Levinstein.¹

Before obtaining a general solution of Eq. (5) for an arbitrary incident atomic current, we will solve it for two special cases, the intensity of the atomic beam incident on the detector being either sine-wave or square-wave modulated. The first one is of interest because it yields a very simple model for the behavior of the ionizer in the frequency domain, while the second one describes our test case when the atomic beam is single-velocity.

If the atomic beam current incident on the ionizer is sine-wave modulated with depth of amplitude modulation d' ,

$$I'(t) = I_0' \left(1 - \frac{d'}{2}\right) + \frac{d'}{2} I_0' \cos \omega t, \quad (6)$$

then the solution to Eq. (5) is given by

$$I_+(t) = \epsilon I_0' \left(1 - \frac{d'}{2}\right) + \frac{\epsilon I_0' d'/2}{(1 + 4\pi^2 v_m^2 \tau^2)^{1/2}} \cos(2\pi v_m t - \theta) \quad (7)$$

where $\theta = \arctan 2\pi v_m \tau$. This shows that in the frequency domain the ionizer behaves as a simple low pass filter of cutoff frequency $v_{co} = 1/2\pi\tau$; the depth of amplitude modulation in the ion signal is given by

$$d_+ = d' / (1 + 4\pi^2 v_m^2 \tau^2)^{1/2}. \quad (8)$$

When the atomic beam current incident on the ionizer is square-wave modulated, as described by Eqs. (1a) and (1b), the solution to Eq. (5) is

$$I_+(t) = \epsilon I_0' \left\{1 - d' \Xi \exp\left[-\frac{t - nT_m}{\tau}\right]\right\} \quad nT_m \leq t < (n+1/2)T_m \quad (9a)$$

$$I_+(t) = \epsilon I_0' \left\{1 - d' + d' \Xi \exp\left[-\frac{t - (n+1/2)T_m}{\tau}\right]\right\} \quad (n+1/2)T_m \leq t < (n+1)T_m \quad (9b)$$

where $\Xi = [1 + \exp(-T_m/2\tau)]^{-1}$. The depth of amplitude modulation in the ion signal is now given by

$$d_+ = \frac{1 - \exp(-1/2 v_m \tau)}{1 + \exp(-1/2 v_m \tau)} d' \quad (10)$$

Eqs. (8) and (10) show clearly the role of the ionic dwell time τ on the degradation of the time-dependent component of the signal. This is also illustrated in Fig. 2.

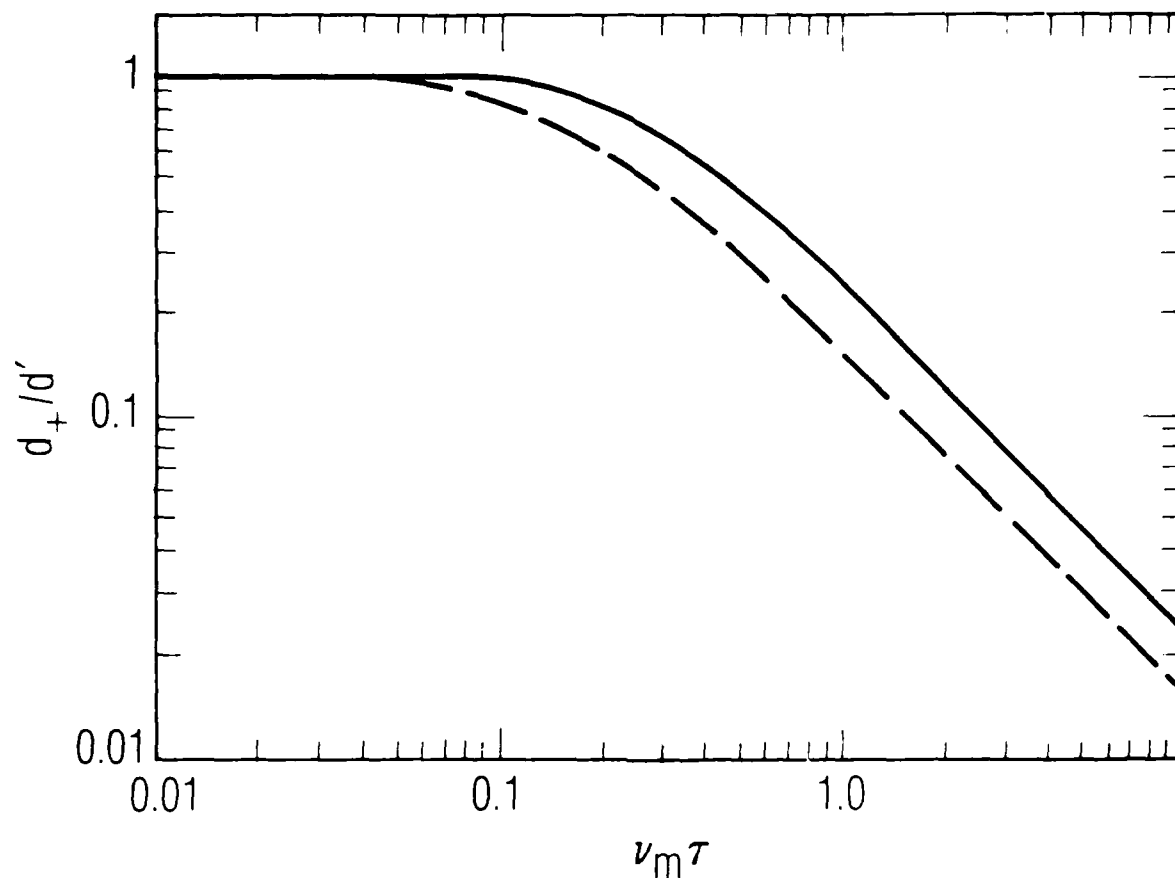


Fig. 2. Response of Ionizer to an Incident Amplitude-Modulated Atomic Beam. Adimensional abscissa: modulation frequency times ionic dwell-time. Adimensional ordinate: ratio of ion current to incident atomic current modulation depths. Solid line: Square-wave modulation. Dashed line: Sine-wave modulation.

A general solution to Eq. (5) can be obtained using Green's function for the problem, $G(t,t')$:

$$I_+(t) = \epsilon \int_{-\infty}^{\infty} G(t,t') I'(t') dt' \quad (11)$$

It is easy to show that $G(t,t')$ is given by

$$G(t,t') = 0 \quad t < t' \quad (12a)$$

$$G(t,t') = \frac{1}{\tau} \exp [-(t-t')/\tau] \quad t \geq t' \quad (12b)$$

and then, for an arbitrary atomic beam incident on the detector,

$$I_+(t) = \frac{e^{-t/\tau}}{\tau} \int_{-\infty}^t e^{t'/\tau} I'(t') dt' \quad (13)$$

III. WAVEFORM DISTORTION

Audoin et al.³ have discussed in detail the effects of the atomic velocity distribution on the frequency stability of optically pumped, optically detected, cesium beam frequency standards, including the effect on the error signal of the spread in atomic transit times between the exit of the Ramsey cavity and the detection region. Similar effects must be incorporated into our analysis of waveform distortion effects in compact cesium beam tubes.

Let $dN_v = I(t') g(v)dv$ be the number of atoms with speeds between v and $v+dv$ in the amplitude-modulated beam passing per unit time through a given cross section of the tube of trajectories leading to the ionizer. The state-selecting and analyzing magnets transmit a normalized atomic beam speed distribution $g(v)$. The same atoms will arrive at the detector at time $t = t' + \bar{t}_A (\bar{v}/v)$, where \bar{v} and \bar{t}_A are the average atomic speed and transit time, respectively. The atomic beam current impinging on the ionizer at time t will be given by

$$I'(t) = \int_0^{\infty} I(t - \bar{t}_A \bar{v}/v) g(v) dv \quad (14)$$

This result can be inserted in Eq. (13) to obtain the ion current out of the ionizer. If we assume phase-sensitive detection with a properly phased square-wave reference signal, the magnitude of the corresponding error signal can be calculated using Eq. (2).

The above procedure gives a full prescription to calculate the error signal provided by the cesium beam tube for any given atomic beam amplitude modulation, assuming that the atomic speed distribution $g(v)$ and the ionizer response parameters ϵ and τ are known. We have used it for our test-case atomic beam, with initial square-wave intensity modulation as given by Eqs. (1a) and (1b). We assume the velocity distribution to be Gaussian, of average \bar{v} and standard deviation σ . Existing measurements^{4,5} of velocity distributions in cesium-beam tubes show results which are somewhat asymmetric, with a high-velocity component extending beyond the Gaussian tail, but we chose a Gaussian representation of $g(v)$ for ease of calculation. The presence of the high velocity components would not change appreciably the results of the present work.

Numerical integration of Eqs. (14) and (13) yields the waveforms into and out of the ionizer. Figure 3 presents the results for the following parameters: $\nu_m = 440$ Hz, $d = 1$, $\bar{t}_A = 1.4 \times 10^{-2}$ s, $\bar{v} = 114$ m/s, $\sigma = 10$ m/s, $\epsilon = 1$ and $\tau = 3 \times 10^{-4}$ s. It shows clearly that in this case, while the effects of the atomic beam velocity spread are quite apparent, the distortion of the ion current waveform relative to the initial atomic beam waveform is dominated by the exponential character of the ionizer emission. Figure 4 shows the corresponding waveforms for $\sigma = 30$ m/s, all other parameters being the same. In this case, velocity-spread effects dominate waveform distortion.

Once the ion current waveform has been determined, Eq. (2) can be used to calculate the detected error signal. Figure 5 shows that for the set of parameters described above, the magnitude of the relative error signal, $|E|/I_0$, is quite insensitive to the atomic beam velocity spread for very narrow speed distributions ($\sigma \leq 4$ m/s), but as the velocity spread increases, $|E|/I_0$ decreases steadily. Figure 6 shows that, as we stated before, these results scale linearly with the amplitude modulation depth d .

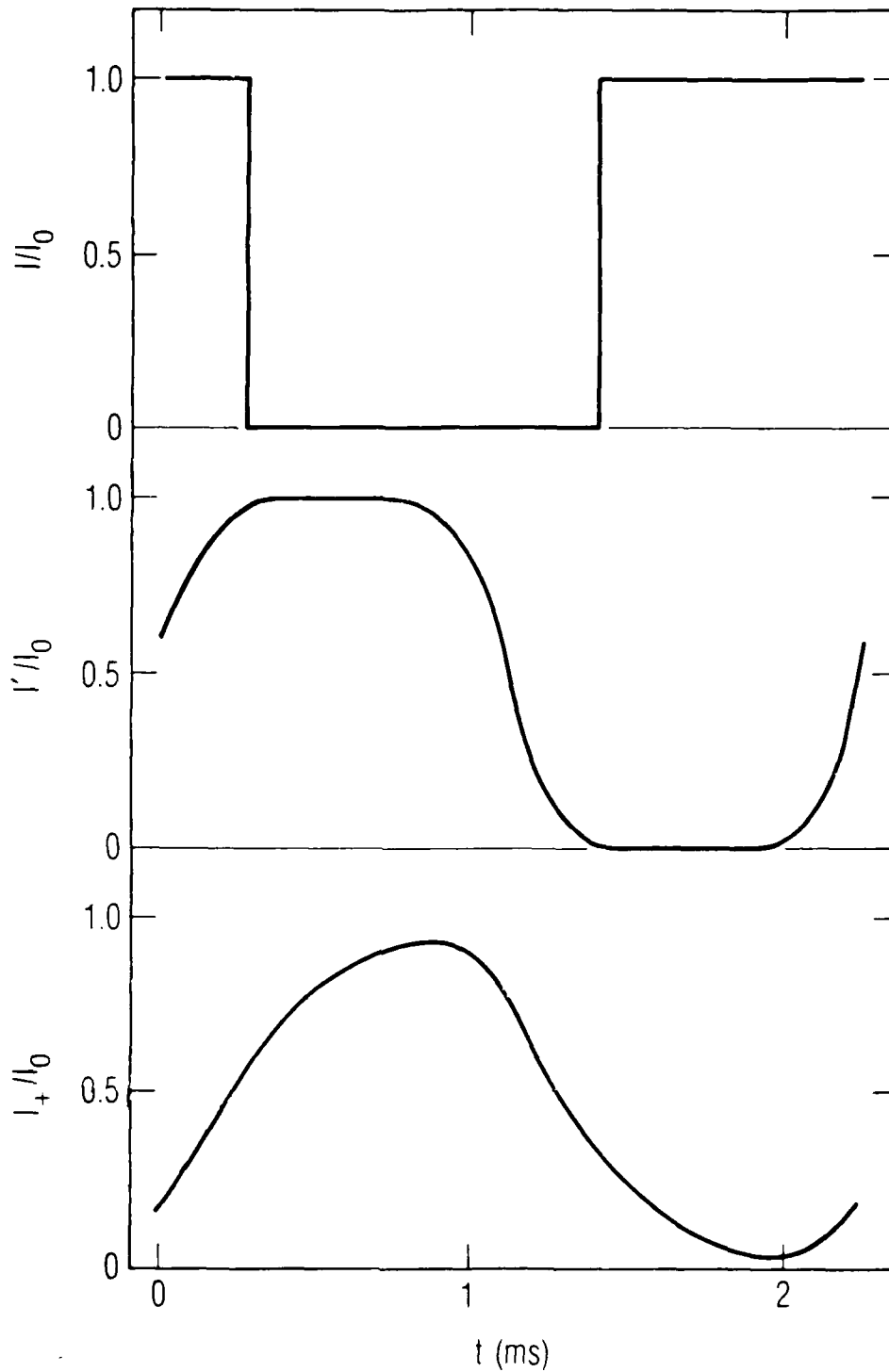


Fig. 3. Amplitude-modulated Waveforms, Normalized by I_0 .
 Top: Initial atomic beam square-wave modulation.
 Middle: Atomic beam incident on ionizer. Bottom:
 Ion current. $v = 114$ m/s, $\sigma = 10$ m/s, $\tau_A = 1.4 \times 10^{-3}$ s, $\nu_m = 440$ Hz, $\tau = 3 \times 10^{-4}$ s, $d = 1$, $\epsilon = 1$.

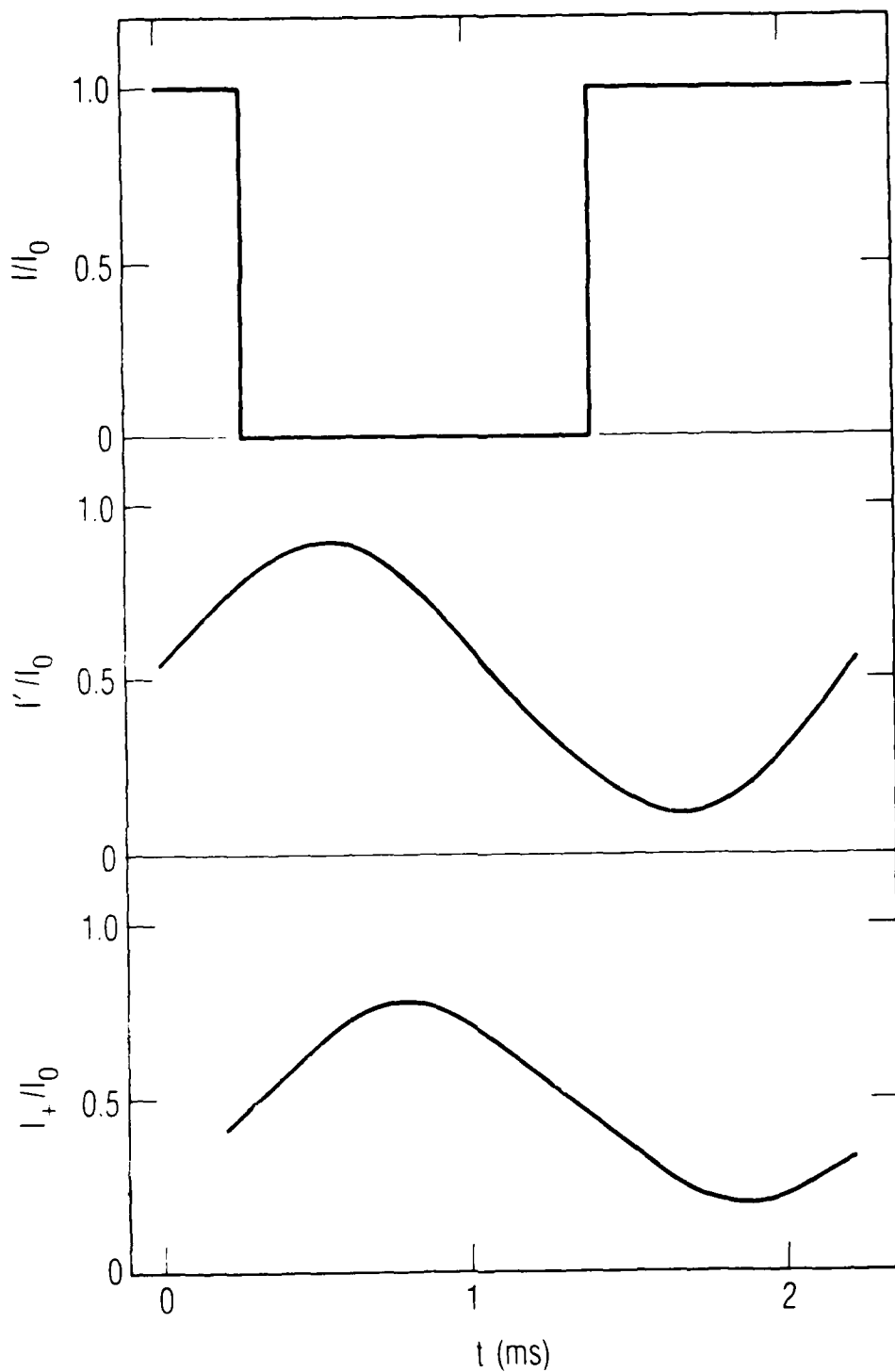


Fig. 4. Amplitude-modulated Waveforms, Normalized by I_0 .
 Top: Initial atomic beam square-wave modulation.
 Middle: Atomic beam incident on ionizer. Bottom:
 Ion current. $\bar{v} = 114$ m/s, $\sigma = 30$ m/s, $t_A = 1.4 \times 10^{-3}$ s,
 $\nu_m = 440$ Hz, $\tau = 3 \times 10^{-4}$ s, $d = A_1$, $\epsilon = 1$.

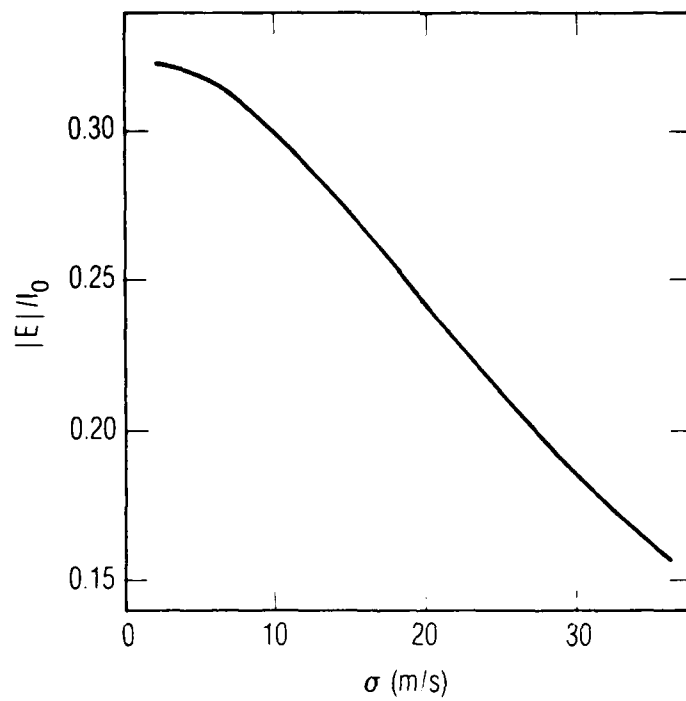


Fig. 5. Magnitude of Detected Error Signal per Unit Beam Intensity vs. Width of Velocity Distribution. $\bar{v} = 114$ m/s, $\tau_A = 1.4 \times 10^{-3}$ s, $\nu_m = 440$ Hz, $\tau = 3 \times 10^{-4}$ s, $d = 1$, $\epsilon = 1$.

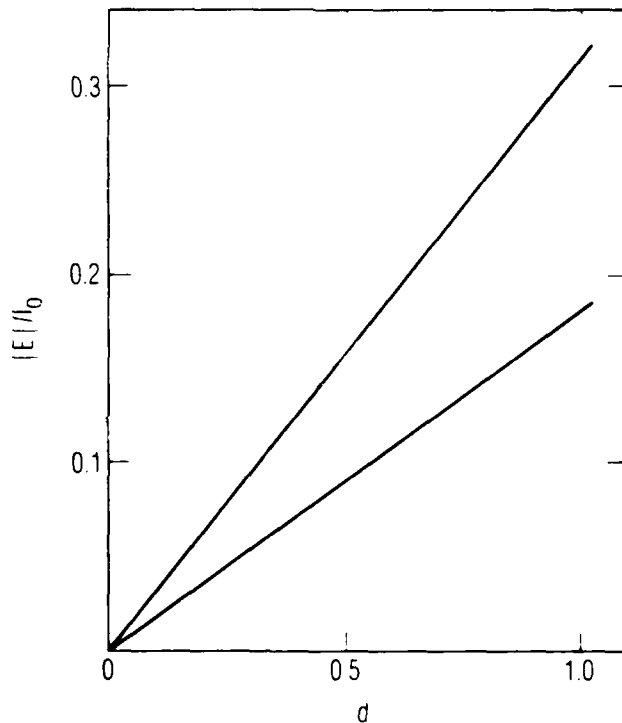


Fig. 6. Magnitude of Detected Error Signal per Unit Beam Intensity vs. Depth of Beam Amplitude Modulation. $\bar{v} = 114$ m/s, $\tau_A = 1.4 \times 10^{-3}$ s, $\nu_m = 440$ Hz, $\tau = 3 \times 10^{-4}$ s, $\epsilon = 1$. Upper trace: $\sigma = 4$ m/s. Lower trace: $\sigma = 30$ m/s.

IV. INTENSITY EFFECTS

From the point of view of the cesium-clock's performance and frequency stability, the quantities of interest in the present work are the error signal S and the signal-to-noise ratio (S/N) . The error signal will be proportional both to (E/I_0) , the relative error signal discussed in the preceding section, and I_0 . We have shown that (E/I_0) decreases as the velocity spread increases, due to waveform distortion. Generally, however, as the velocity spread increases, I_0 will increase too, making it necessary to analyze in more detail the behavior of their product, $(E/I_0)I_0$. With regard to the signal-to-noise ratio, if we assume that the atomic beam is shot-noise limited, the noise level within the measurement bandwidth will be proportional to $I_0^{1/2}$, so that the signal-to-noise ratio will be proportional to $(E/I_0)I_0^{1/2}$.

Let $\phi(v)$ be the atomic beam intensity per unit speed interval within the tube of trajectories leading to the ionizer prior to velocity selection. If we assume the speed distribution of the cesium atoms effusing out of the oven to be beam-Maxwellian,

$$\phi(v) = \frac{2\phi_0}{\alpha} \left(\frac{v}{\alpha}\right)^3 \exp [-(v/\alpha)^2] \quad (15)$$

where $\alpha = (2kT/m)^{1/2}$; m is the mass of a cesium atom, T the absolute oven temperature, and ϕ_0 the atomic beam intensity within the tube of trajectories leading to the ionizer prior to velocity selection. As I_0 is the corresponding intensity after velocity selection, assuming unit transmission at the transmitted peak of the velocity distribution, $v = v_0$, it follows that $\phi(v_0) dv = I_0 g(v_0) dv$, which results in $I_0 = \phi(v_0)g/(v_0)$. For our choice of a Gaussian velocity distribution, $v_0 = \bar{v}$ and

$$I_0 = \sqrt{8\pi} \phi_0 \frac{\sigma}{\alpha} \left(\frac{\bar{v}}{\alpha}\right)^3 \exp [-(\bar{v}/\alpha)^2]. \quad (16)$$

Equation (16) shows that for a given oven temperature and fixed average speed, \bar{v} , I_0 will be proportional to the Gaussian's standard deviation σ . From the analysis at the beginning of this section, it follows that the error signal will be proportional to $(E/I_0) \sigma$ and the signal-to-noise ratio will be

proportional to $(E/I_0) \sigma^{1/2}$. In both cases the first factor (E/I_0) reflects the effect of waveform distortion, while the second one (σ or $\sigma^{1/2}$) introduces beam intensity effects.

The results shown in Fig. 7 were obtained using the same set of parameters used in the previous section, and illustrate for our test case the results of the two competing effects described in this section. For relatively narrow speed distributions (up to $\sigma \approx 18$ m/s in our test case), intensity effects are dominant and the signal increases quasi-linearly with increasing velocity spread. For broader speed distributions, waveform distortion effects become dominant, and the signal saturates against further increases in velocity spread. The signal-to-noise ratio shows a maximum at $\sigma \approx 18$ m/s and then decreases slowly with increasing σ when waveform distortion effects become dominant.

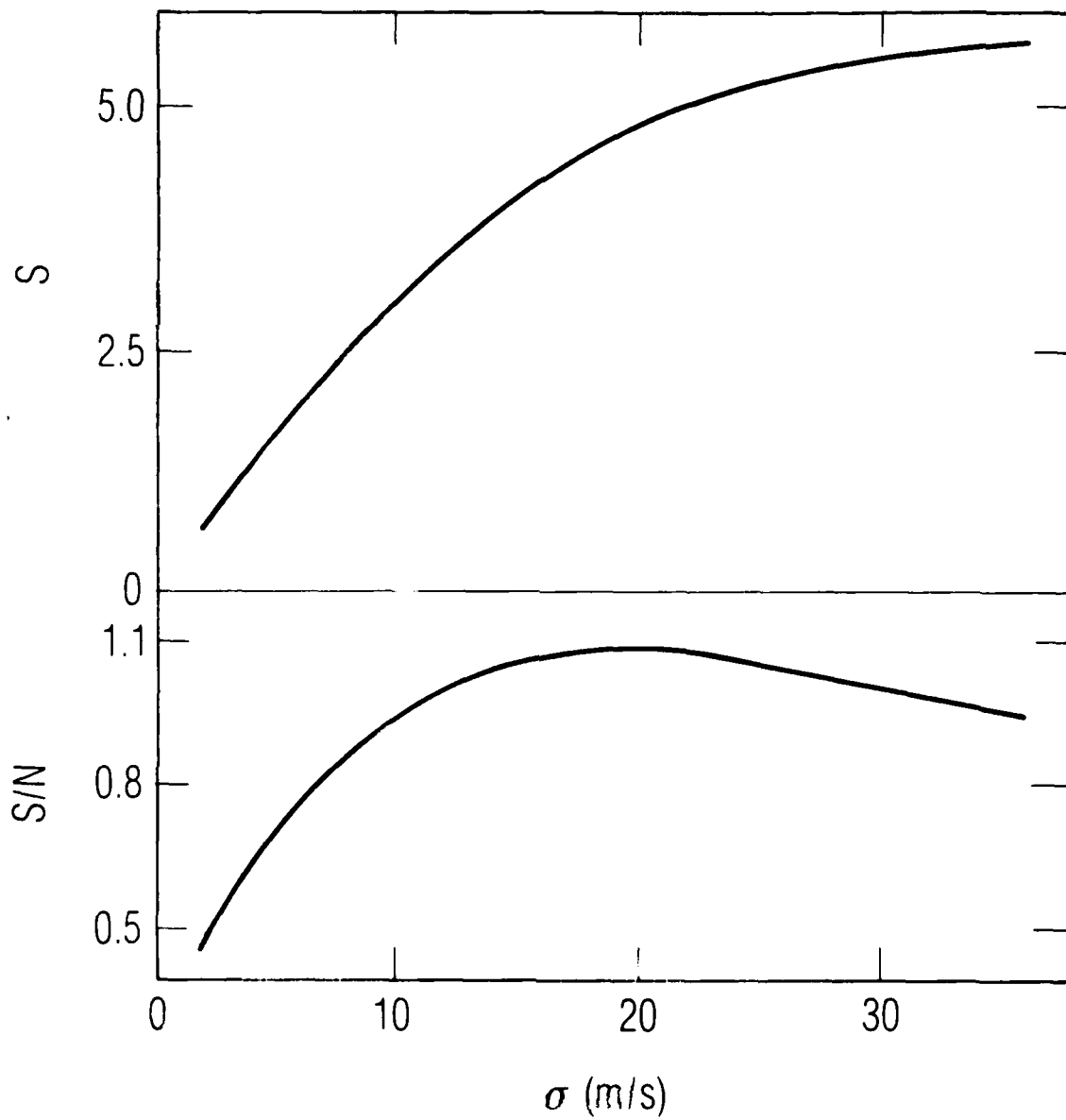


Fig. 7. Signal (top) and Signal-to-Noise Ratio (bottom) (in arbitrary units) vs. Width of Velocity Distribution. $\bar{v} = 114$ m/s, $t_A = 1.4 \times 10^{-3}$ s, $v_m = 440$ Hz, $\tau = 3 \times 10^{-4}$ s, $d = 1$, $\epsilon = 1$.

V. CONCLUSIONS

We have shown that the distribution of atomic arrival times at the cesium beam tube ionizer, as well as the distribution of ionic residence times on the ionizer surface, affect the performance of a cesium beam tube by distorting the time-dependence of the cesium ion current relative to the amplitude modulation impressed on the state-selected atomic beam by the combination of microwave interrogation and state analysis. This distortion results in a reduction of the error signal relative to the average ion current, and thus leads to degradation of the clock's discriminator function. The spread in atomic arrival times is, of course, related to the width of the atomic velocity distribution. Increasing it will increase the atomic-beam intensity and thus the magnitude of the error signal, but as it becomes broader, the degradation due to waveform distortion may become dominant.

Figure 8 presents the frequency response of the post-microwave segment of a cesium beam tube for $\epsilon = 1$, $d = 1$, $\bar{v} = 114$ m/s and $\bar{t}_A = 1.4 \times 10^{-3}$ s. For a single-velocity beam and prompt ionization ($\tau = 0$), $|E|/I_0 = 1/2$, independent of modulation frequency, as illustrated by the dotted line. If now the ionizer exponential distribution of residence times is incorporated, Eqs. (2), (9a) and (9b), combined with $\langle I_+ \rangle = I_0/2$, yield

$$\frac{|E|}{I_0} = \frac{1}{2} - 2v_m t^* + 2v_m \tau [1 - 2\epsilon \exp(-t^*/\tau)] \quad (17)$$

where $t^* = \tau \ln(2\epsilon)$. This result is indicated by the dashed line. The solid line shows the effect of replacing the single-velocity atomic beam by one having a Gaussian distribution of $\sigma = 10$ m/s. In this particular case, the main effect of the velocity spread in the atomic beam is to force a much sharper signal cut-off as the modulation frequency increases.

In light of these results, the main conclusion of this report is that, when determining the frequency-modulation scheme, attention should be paid not only to the atomic interaction with the microwave field in the Ramsey cavities, but also to these "post-microwave segment" effects. As shown in Fig. 8, the waveform distortion effects discussed here can be minimized by choosing an appropriate operating point on the frequency-response curve of the post-microwave segment of the cesium beam tube.

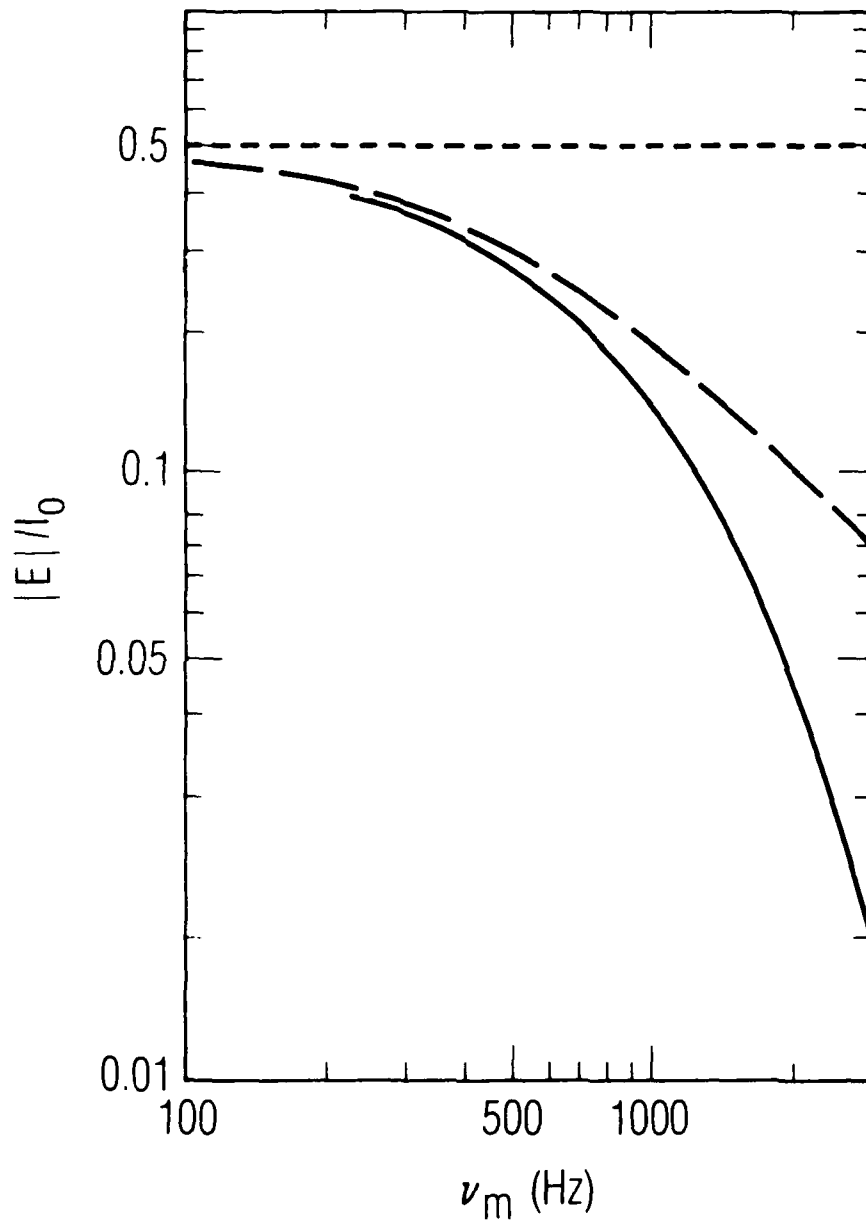


Fig. 8. Magnitude of Detected Error Signal per Unit Beam Intensity vs. Modulation Frequency. $\bar{v} = 114$ m/s, $t_A = 1.4 \times 10^{-3}$ s, $d = 1$, $\epsilon = 1$. Dotted line: no distortion. Dashed line: single-velocity beam, $\tau = 3 \times 10^{-4}$ s. Solid line: $\sigma = 10$ m/s, $\tau = 3 \times 10^{-4}$ s.

While the present analysis has been developed for compact cesium beam tubes using surface ionization detectors, some of its conclusions are valid for other atomic beam passive-frequency standards. They are particularly significant in light of the current push to use diode lasers (rather than magnets) to prepare and analyze the hyperfine state of the cesium beam by optical means. In that case, the full Maxwellian distribution of velocities may contribute to the signal, and careful attention must be paid to the modulation scheme to avoid excessive signal-to-noise losses due to waveform distortion, as recently discussed by Audoin et al.³.

REFERENCES

1. F. L. Hughes and H. Levinstein, "Mean Adsorption Lifetime of Rb on Etched Tungsten Single Crystals: Ions," Phys. Rev., 113, pp. 1029-1035 (1958).
2. E. G. Nazarov, "Observation of Atomic Desorption Dynamics with a Voltage-Modulation Method," Sov. Phys. Tech. Phys. 24, pp. 707-710 (1979). (Transl. from Zh. Tekh. Fiz., vol. 49, pp. 1277-1281, 1979).
3. C. Audoin, V. Candelier and J. Vanier, "Effect of the Atom Transit Time on the Frequency Stability of Cesium Beam Frequency Standards," Proc. 40th Ann. Freq. Control Symposium. New York: IEEE 1986, pp. 432-440.
4. H. Hellwig, S. Jarvis, Jr., D. J. Glaze, D. Halford and H. Bell, "Time Domain Velocity Selection Modulation as a Tool to Evaluate Cesium Beam Tubes," Proc. 27th Ann. Freq. Control Symposium, Washington. Electronic Industries Association, 1973, pp. 357-366.
5. D. A. Howe, "Velocity Distribution Measurements of Cesium Beam Tubes," Proc. 30th Ann. Freq. Control Symposium, Washington. Electronic Industries Association, 1976, pp. 451-456.

LABORATORY OPERATIONS

The Aerospace Corporation functions as an "architect-engineer" for national security projects, specializing in advanced military space systems. Providing research support, the corporation's Laboratory Operations conducts experimental and theoretical investigations that focus on the application of scientific and technical advances to such systems. Vital to the success of these investigations is the technical staff's wide-ranging expertise and its ability to stay current with new developments. This expertise is enhanced by a research program aimed at dealing with the many problems associated with rapidly evolving space systems. Contributing their capabilities to the research effort are these individual laboratories:

Aerophysics Laboratory: Launch vehicle and reentry fluid mechanics, heat transfer and flight dynamics; chemical and electric propulsion, propellant chemistry, chemical dynamics, environmental chemistry, trace detection; spacecraft structural mechanics, contamination, thermal and structural control; high temperature thermomechanics, gas kinetics and radiation; cw and pulsed chemical and excimer laser development including chemical kinetics, spectroscopy, optical resonators, beam control, atmospheric propagation, laser effects and countermeasures.

Chemistry and Physics Laboratory: Atmospheric chemical reactions, atmospheric optics, light scattering, state-specific chemical reactions and radiative signatures of missile plumes, sensor out-of-field-of-view rejection, applied laser spectroscopy, laser chemistry, laser optoelectronics, solar cell physics, battery electrochemistry, space vacuum and radiation effects on materials, lubrication and surface phenomena, thermionic emission, photo-sensitive materials and detectors, atomic frequency standards, and environmental chemistry.

Computer Science Laboratory: Program verification, program translation, performance-sensitive system design, distributed architectures for spaceborne computers, fault-tolerant computer systems, artificial intelligence, microelectronics applications, communication protocols, and computer security.

Electronics Research Laboratory: Microelectronics, solid-state device physics, compound semiconductors, radiation hardening; electro-optics, quantum electronics, solid-state lasers, optical propagation and communications; microwave semiconductor devices, microwave/millimeter wave measurements, diagnostics and radiometry, microwave/millimeter wave thermionic devices; atomic time and frequency standards; antennas, rf systems, electromagnetic propagation phenomena, space communication systems.

Materials Sciences Laboratory: Development of new materials: metals, alloys, ceramics, polymers and their composites, and new forms of carbon; non-destructive evaluation, component failure analysis and reliability; fracture mechanics and stress corrosion; analysis and evaluation of materials at cryogenic and elevated temperatures as well as in space and enemy-induced environments.

Space Sciences Laboratory: Magnetospheric, auroral and cosmic ray physics, wave-particle interactions, magnetospheric plasma waves; atmospheric and ionospheric physics, density and composition of the upper atmosphere, remote sensing using atmospheric radiation; solar physics, infrared astronomy, infrared signature analysis; effects of solar activity, magnetic storms and nuclear explosions on the earth's atmosphere, ionosphere and magnetosphere; effects of electromagnetic and particulate radiations on space systems; space instrumentation.